JOURNAL OF
biomaterials applications

Hard Tissues and Materials

Journal of Biomaterials Applications
2018, Vol. 32(7) 906–919

DOI: 10.1177/0885328217745699
journals.sagepub.com/home/jba
SAGE

Role of geometrical cues in bone marrow-derived mesenchymal stem cell survival, growth and osteogenic differentiation

Dhanak Gupta[1,2], David M Grant[2], Kazi M Zakir Hossain[2], Ifty Ahmed[2] and Virginie Sottile[1]

Abstract

Mesenchymal stem cells play a vital role in bone formation process by differentiating into osteoblasts, in a tissue that offers not a flat but a discontinuous three-dimensional (3D) topography *in vivo*. In order to understand how geometry may be affecting mesenchymal stem cells, this study explored the influence of 3D geometry on mesenchymal stem cell-fate by comparing cell growth, viability and osteogenic potential using monolayer (two-dimensional, 2D) with microsphere (3D) culture systems normalised to surface area. The results suggested lower cell viability and reduced cell growth in 3D. Alkaline phosphatase activity was higher in 3D; however, both collagen and mineral deposition appeared significantly lower in 3D, even after osteogenic supplementation. Also, there were signs of patchy mineralisation in 3D with or without osteogenic supplementation as early as day 7. These results suggest that the convex surfaces on microspheres and inter-particulate porosity may have led to variable cell morphology and fate within the 3D culture. This study provides deeper insights into geometrical regulation of mesenchymal stem cell responses applicable for bone tissue engineering.

Keywords

Mesenchymal stem cells, microspheres, substrate geometry, osteogenesis, 3D culture

Introduction

Mesenchymal stem cells (MSCs) present in the bone marrow take part in bone remodelling by differentiating into bone forming osteoblasts.[1] Since the standard methodology for studying these cells *in vitro* involves culture on a flat surface (as monolayers), current understanding of physiological osteoblastogenesis and bone remodelling may not truly represent the three dimensional *in vivo* environment.[2]

Cells attach to the extracellular matrix (ECM) via integrins, which form a bridge between ECM and the actin-myosin cytoskeleton present inside the cell, thereby enabling bi-directional transmission of forces across the plasma membrane.[3,4] The concept of two-dimensional (2D) and three-dimensional (3D) culture arises on the basis of different patterns of integrin expression in the two culture systems. In 2D (or monolayers), cells adhere to the underlying matrix in one plane and in 3D, adhesion is possible across multiple planes of the same cell.[5] This results in differences in cell morphology, organisation of plasma membrane, cytoskeletal architecture, motility and nucleus structure and position that may ultimately lead to different cell fates via changes in molecular pathways.[5–7]

Effects of 3D culture environments were initially encountered in cancer biology. For example, growth of human breast tumour cells was arrested due to down-modulation of β1-integrin signalling only in 3D basement membrane assay and not in monolayers.[8]

[1]Wolfson Centre for Stem Cells, Tissue Engineering and Modelling (STEM), School of Medicine, University of Nottingham, Nottingham, UK
[2]Advanced Materials Research Group, Faculty of Engineering, University of Nottingham, UK

Corresponding author:
Virginie Sottile, University of Nottingham, CBS Building, Nottingham NG7 2RD, UK.
Email: virginie.sottile@nottingham.ac.uk

More recently Sung et al.[9] demonstrated that human mammary fibroblasts secrete more paracrine factors in 3D than in 2D and these factors are capable of increasing the invasive behaviour of breast cancer cells. The difference between 2D and 3D cell culture systems has also been demonstrated in cell migration. On 2D matrix, cells are known to undergo lamellipodia-based movement, propagated by actomyosin contractility, after polarisation and adhesion of cells to matrix. However, there is another type of cell movement in 3D that is absent in 2D, which is called high-pressure migration. It relies on formation of a high intracellular pressure that is created towards the front of the cell.[10] Bone marrow derived MSCs are responsive to 2D and 3D culture environments, as shown in studies from Maeno et al.[11] demonstrating that differentiation is differently regulated in 2D than 3D systems. One of the commonly used 3D culture system is smooth microspheres (MS), which have been developed in different sizes and with different biomaterials including hydroxyapatite, bioactive glass, polymers for a number of applications such as cancer therapy, large scale cell-expansion and as injectable materials for drug or cell delivery in tissue regeneration.[12–15] In this study, the growth, viability and osteogenic fate of bone marrow derived-MSCs were compared on monolayer format (referred to as 2D) and on MS (referred to as 3D geometry) with similar surface areas, using spheres of known radii of curvature in both normal as well osteogenic induction media. This study presents original data comparing cell culture efficiency in 2D and 3D models using a defined MSC seeding density normalised to surface area, which suggest that the convex surfaces on MS and inter-particulate porosity may lead to variable cell morphology and fate within the 3D culture. This study provides deeper insights into geometrical regulation of MSC responses, and suggests that bone surface may trigger cytoskeletal changes and thus, early osteogenesis *in vivo*.

Materials and methods

Reagents used were purchased from Thermo Fisher Scientific (UK) unless otherwise stated.

Preparation of borosilicate glass microspheres (BSG)

Borosilicate glass (Samco, UK) was ground into particles using a Retsch PM100 milling machine. These particles were then sieved into the size range of interest (63–150 μm) and flame-spheroidised in an oxyacetylene flame utilising a flame spray gun (Metallisation Ltd, UK).[16] The resulting spherical particles thus collected (borosilicate glass microspheres, BSG), were used as 3D culture system. The BSG had major axis length ranging from 8 to 270 μm (mean ± standard deviation (S.D.): 90 ± 47 μm) and sphericity ranging from 0.1 to 1.0 (mean ± S.D.: 0.8 ± 0.2 μm), measured using image analysis (Image J)[17] of scanning electron microscopy (SEM) images of BSG (see Supplementary Figure 1). BSG had a chemical composition of B_2O_3-SiO_2-Na_2O-Al_2O_3-CaO at 9.5%-82.0%-5.5%-2.0%-1.0% with measurement error of 2%, measured using elemental dispersion X-ray spectroscopy analysis. Borosilicate was used as the choice of material for this study as it is known to be non-degradable under physiological conditions and does not release any bioactive substances that can affect cell fate.[18] This allowed assessment of 2D vs. 3D without interference from any inductive/toxic factors that may be released in case of other biodegradable materials.[19]

Human mesenchymal stem cell culturing

Adult human bone marrow-derived immortalised mesenchymal stem cells (hMSCs)[20–22] and Green Fluorescent Protein (GFP) expressing hMSCs were used[23] in this study as previously described. Live cell images were taken using JuLI™ FL (NanoEnTek, Korea).

The cells were cultured in standard culture (SC) medium containing Dulbecco's Modified Eagle Medium (DMEM) supplemented with 10% (v/v) foetal calf serum (FCS), 1% (v/v) non-essential amino acids, 1 mM L-glutamine and 0.5% (v/v) Penicillin/Streptomycin, and maintained at 37°C in humidified atmosphere with 5% CO_2. At 70–90% confluency, the culture medium was removed; cells were then washed with phosphate saline buffer (PBS) and then harvested using 0.05% Trypsin-EDTA.

Cell seeding

In order to grow cells in 2D, glass coverslips (made from D263M borosilicate glass with chemical composition of B_2O_3-SiO_2-Na_2O-Al_2O_3-K_2O-ZnO-TiO_2-Sb_2O_3 at 8.4%-64.1%-6.4%-4.2%-6.9%-5.9%-4.0%-0.1% and supplied by SLS, UK) were added to each well in a non-tissue culture-treated 24-well plate (2 cm^2 per well). For 3D culturing, BSG were weighed to provide a constant surface area of 2 cm^2 (unless otherwise mentioned) by first measuring the tapped density of BSG and then nominalising to a nominal size distribution of 100 μm, followed by cleaning with IMS (Industrial Methylated Spirit, SLS, UK) for 2 h at constant agitation at 30 RPM, before air-drying overnight in cell culture hood. Particles were then washed three times with PBS and three times with SC medium, before a 30 min incubation at room temperature (RT) in SC medium. BSG in medium were transferred to wells previously coated with 100 μl of

pHEMA (poly(2-hydroxyethyl methacrylate), Sigma–Aldrich, UK) solution at 10 mg/ml in 95% ethanol, to provide ultra-low cell attachment conditions.[24] The BSG formed a single layer at the bottom of the well. Finally, the medium was carefully removed and replaced with the cell suspension (200 µl per well in 3D and 500 µl per well in 2D). 3D samples were further agitated at 45 RPM for 5 min at RT, followed by a 30-min static incubation at 37°C and 5% CO_2. This regime was repeated five times before undisturbed incubation overnight at 37°C and 5% CO_2.[16,25] Medium change was performed 24 h after cell seeding and subsequently every 2–3 days for the length of experiment.

Osteogenic differentiation

For osteogenic differentiation, 24 h after hMSC seeding (considered as Day 0 of differentiation), medium was changed to either fresh SC medium or osteogenic stimulation (OS) medium. The OS medium was made by supplementing the SC medium with 100 nM dexamethasone (Sigma–Aldrich, UK), 10 mM β-glycerophosphate (Sigma–Aldrich, UK) and 0.05 mM L-ascorbic acid-2-phosphate (Sigma–Aldrich, UK).[22] Subsequently, medium changes were performed every 2–3 days for up to three weeks of culture.

DNA assay

All samples were lysed by three cycles of freeze thawing at –80°C. The 3D samples were further sonicated using Bioruptor®, Diagenode, USA. The cell lysates ($n \geq 3$) were then diluted (1 in 100 in Tris-EDTA buffer) and 100 µl of samples was added to a flat 96-well plate. DNA content was quantified using Quant-iTM PicoGreen® dsDNA Assay kit according to manufacturer's instruction. Florescence intensity readings were taken on a Tecan Infinite M200 microplate reader (Tecan, UK) at 480 nm excitation and 520 nm emission. The DNA concentration was extrapolated using a standard curve prepared from calf thymus standard DNA provided with the assay kit.

Cell metabolic activity assay

To measure cell metabolic activity, a PrestoBlue® assay was performed. Briefly, medium was removed and cells were washed with PBS before adding PrestoBlue® working solution (1:9 Reagent:warm Hanks Balanced Salt Solution (HBSS)) to each test well ($n \geq 3$) and three blank wells. The volume of working solution added to each test well was equal to the volume of culture medium initially present. Cells were then incubated at 37°C and 5% CO_2 until colour change according to manufacturer's instructions. Then 100 µl of reaction solution was transferred to a clear 96-well plate and fluorescence reading was measured at 530 nm excitation and 590 nm emission filters on a Tecan Infinite M200 microplate reader. Cell metabolic activity was expressed after subtracting the reading for unreduced (blank) reagent and normalising to the reaction time.

Scanning Electron Microscopy (SEM)

The 3D samples were first fixed in 4% PFA (paraformaldehyde, VWR Chemical, UK) in PBS (at 4°C) and then incubated in 100 µl/well of 1% Osmium tetroxide (Sigma–Aldrich, UK) for 45 min at RT, followed by dehydration by washing with increasing concentrations of ethanol (20%, 40%, 60%, 70%, 80%, 90% and up to 100%) and finally, Hexamethyldisilazane (HMDS, Sigma–Aldrich, UK) for approximately 5 min each. After washes, the samples were mounted on Aluminium stubs using Carbon adhesive tabs and left overnight in HMDS, to air dry in a fume hood. The following day, samples were sputter-coated in platinum and secondary electron images were acquired using Philips (FEI) XL(30)-wXL^{30}-w SEM at electron beam of 5–10 kV. The 3D agglomerates were also sectioned into two halves using a fine spatula, without penetrating or touching the inside of the agglomerate. The sectioned samples were again coated with platinum before visualising under SEM.

Fluorescein diacetate (FDA)/propidium iodide (PI) staining

At each time point, cells were washed with PBS, and then DMEM containing 8 µg/ml FDA (Merck Millipore, UK) and 20 µg/ml PI (Sigma–Aldrich, UK) was added.[26] Cells were incubated at RT for 5 min in the dark, then after removing DMEM containing dyes, fresh DMEM only was added for imaging. Images were acquired using a Nikon TS100 Inverted fluorescent microscope with filters for Texas Red and FITC. Images ($n \geq 4$) were used to quantify red and green fluorescence signals on days 1 and 4 of culture using Image J. Percentage cell viability was calculated by dividing the green pixels by total pixels (green + red) in the same field of view.

Alkaline phosphatase (ALP) activity

ALP activity was measured using SIGMAFAST™ p-Nitrophenyl phosphate tablets (substrate) (Sigma–Aldrich, UK). Briefly, 100 µl of cell lysates (or sterile distilled water for three blank wells) and 100 µl of substrate were added to each assay well and absorbance at 405 nm was measured on Tecan Infinite M200

microplate reader every 3 min upto 2 h, to identify the kinetic phase of the reaction. The ALP activity is expressed as absorbance/min/μg of DNA ($n \geq 3$) after removing background.

Sectioning of 3D agglomerates

After removing culture medium, 3D agglomerates were fixed in 4% PFA in PBS (at 4°C) for 10 min, washed with PBS for 5 min, followed by immersion in sucrose solution, until the agglomerates sank. The samples were then transferred to a custom mould, embedded in OCT medium (VWR Chemical, UK) and stored in −20°C until sectioning.

Agglomerates were cryosectioned and 20 μm sections were collected on slides, air-dried overnight at RT and stored at 4°C. These sections were used to perform Sirius Red staining and Haematoxylin and Eosin (H&E) staining (Supplementary Figure 2).

Sirius Red staining

For staining, a working solution of 0.1% Sirius Red (Sigma–Aldrich, UK) was prepared in saturated picric acid (Sigma–Aldrich, UK).[27,28] For qualitative assessment, monolayers on coverslips and 3D-cryosections were incubated in Sirius Red working solution for 30 min with occasional agitation. In case of 3D cryosections, the excess stain was removed by blot drying and mounted using DPX (Dibutyl Phathalate Xylene, Sigma–Aldrich, UK) before visualising under an ECLIPSE 90i Nikon Microscope. In case of 2D, imaging was performed using a Nikon Eclipse TS100, after washing with sterile distilled water to remove excess stain in the well plates. Mouse calvarial tissue was used as a positive control for collagen staining.

For quantification assessment, intact 3D agglomerates or 2D coverslips ($n \geq 3$) were used. Fixed samples were incubated with Sirius Red for 30 min at RT with occasional agitation, washed with sterile distilled water and incubated with de-staining solution (1:1 0.1 N NaOH:Methanol) for 30 min, before using 100 μl to measure OD at 540 nm using a Tecan Infinite M200 microplate reader. The background was subtracted using the absorbance readings of three blank wells and total collagen per sample was extrapolated using a standard curve prepared from rat tail collagen type 1 (Sigma–Aldrich, UK).

Alizarin Red staining

Cells were washed three times with PBS and fixed in 4% PFA in PBS (at 4°C) for 15 min before staining with 1% Alizarin Red solution for 10 min at RT with occasional agitation. Excess stain was removed with distilled water. For 3D samples, the agglomerates were crushed slightly using a fine spatula before imaging. For quantification analysis, stained samples were incubated in de-staining solution (20% methanol and 10% acetic acid in dH_2O) for 15 min, before 100 μl were used to measure OD at 540 nm using a Tecan Infinite M200 microplate reader ($n \geq 3$). Calcium deposition was expressed as absorbance units after subtracting background using three blank wells, and normalising to the initial volume of de-staining solution added and to DNA content.

H&E staining

To study the extent of ECM formation in 3D, GFP-labelled hMSCs were seeded at 10,000 cells/cm^2 and cultured in SC and OS medium. On day 21 of differentiation, 3D cryosections were stained in H&E.[29] The samples were dehydrated and mounted with DPX before imaging under an ECLIPSE 90i Nikon Microscope. Mouse calvarial tissue was used as control.

Statistical analyses

All statistical analyses were performed using IBM SPSS Statistics 22. Mean, S.D. and standard errors were computed for at least three replicate samples in all experiments. For all investigations, except calcium deposition, two-way ANOVA was performed with days and culture condition as two fixed factors. For quantitative assessment of calcium deposition, one-way ANOVA was performed with culture condition as a fixed factor. For pairwise comparisons, post-hoc analyses using Least Significant Difference (LSD, equivalent to no adjustments) were carried out. P values < 0.05 were considered significant. ANOVA was performed after testing for data normality using a Shapiro–Wilk test.

Results

Cell attachment

For the assessment of cell attachment, GFP-labelled hMSCs were seeded at 625, 1250, 2500, 5000 and 10,000 cells/cm^2 and after 24 h, cell metabolic activity and DNA measurements were performed. The cell metabolic assay results (Figure 1(a)) showed higher activity in 3D than in 2D at cell seeding densities 2500, 5000 and 10,000 cells/cm^2, respectively ($p < 0.001$). DNA quantification for same biological replicates (Figure 1(b)) confirmed higher DNA content in 3D compared to 2D at higher cell seeding densities of 5000 and 10,000 cells/cm^2 ($p < 0.001$).

Live cell fluorescent imaging 24 h after cell seeding (Figure 1(c)) indicated that there was aggregate

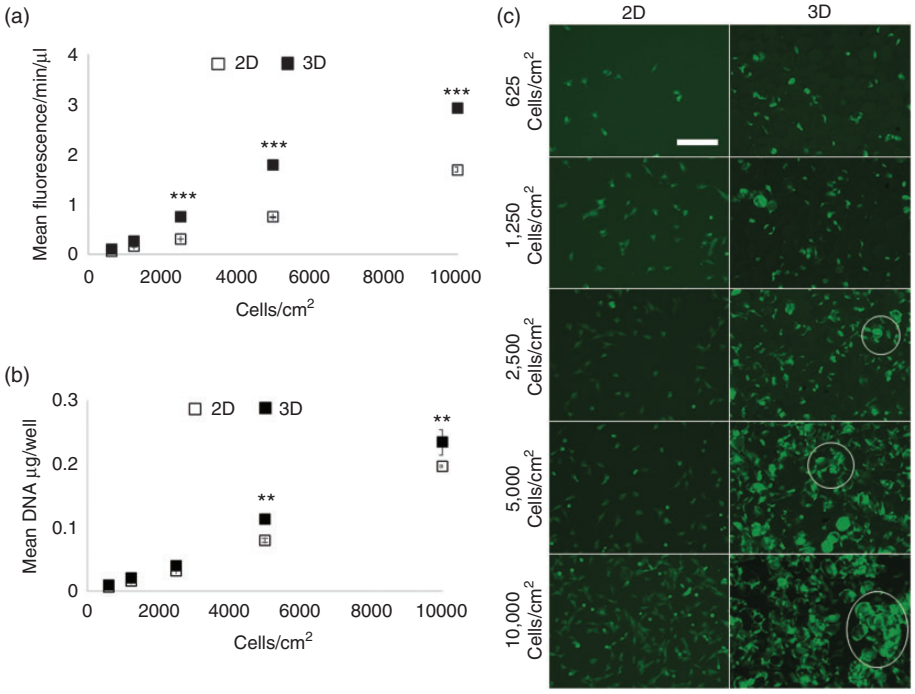

Figure 1. Cell attachment of human mesenchymal stem cells 24 h after seeding in 2D and 3D cultures. Cells were seeded at 625, 1250, 2500, 5000 and 10,000 cells/cm^2. (a) Cell metabolic activity, (b) DNA content assay and (c) representative fluorescent channel images taken on day one of culture. Aggregate formation is highlighted in white circles. $^{**}p < 0.01$, $^{***}p < 0.001$ between 2D and 3D at same time point, n = 3, error bars represent S.E.M. Scale bar – 250 µm.

formation in 3D at higher densities, and these aggregates seemed to form as a result of cells present in interparticulate regions, bridging across from one MS to another.

Cell proliferation

To investigate the effects of 2D and 3D culture on cell proliferation, GFP-labelled hMSCs were seeded at 2500 cells/cm^2 and DNA and cell metabolic activity measurements were performed over 42 days of culture. The results (Figure 2(a) and (b)) showed that there was significantly higher DNA content and metabolic activity in 2D compared to 3D after 4 days of culture and beyond, despite same surface area available for growth in both conditions ($p < 0.001$). This indicated lower proliferative activity in 3D than in 2D. Using, the DNA content measurements on day 31 of culture, it was calculated that 3D contained only 23% of the cells as compared to in 2D, which indicated that cells in 3D possibly occupied only 23% of the surface area provided for cell proliferation.

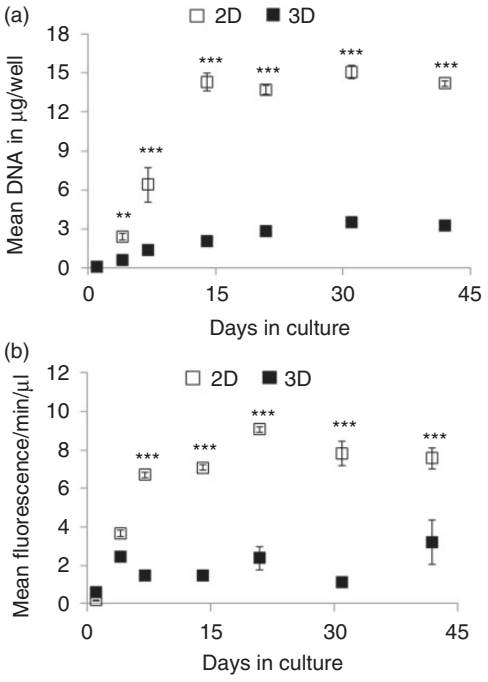

Figure 2. Growth of human mesenchymal stem cells in 2D and 3D after cell seeding at 2500 cells/cm^2. DNA and cell metabolic activity measurements were performed over 42 days. $^{**}p < 0.01$, $^{***}p < 0.001$, compared to other condition on same time point, n = 3, error bars represent S.E.M.

Heterogeneity in 3D system

To investigate reasons for reduced cell proliferation of hMSCs in 3D, SEM was carried out and the images of typical 3D agglomerate have been shown in Figure 3(a)

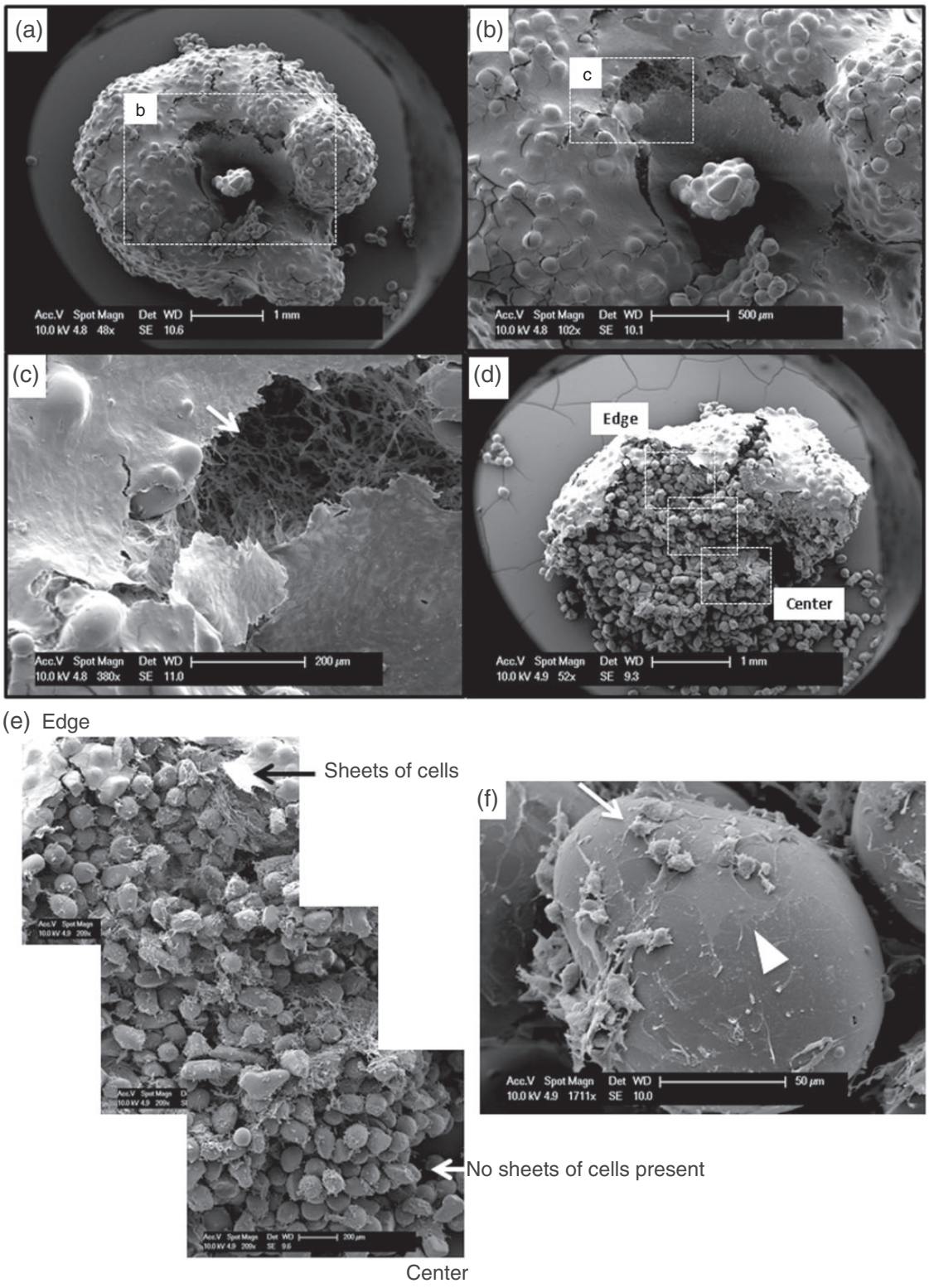

Figure 3. Scanning electron microscopy images of 3D agglomerates on Day 14 after cell seeding at 167 cells/cm^2. Increasing magnification images (a–c) of intact 3D agglomerate showed cells covering the entire agglomerate in multiple layers (arrow). This agglomerate (d) was sectioned and images of cells were acquired from three internal regions (e). There seemed to be more cells near the edges of the agglomerate compared to central regions (arrows in e). Also, note the presence of both rounded cells (arrows) and flat cells (arrow heads, f) in the sample.

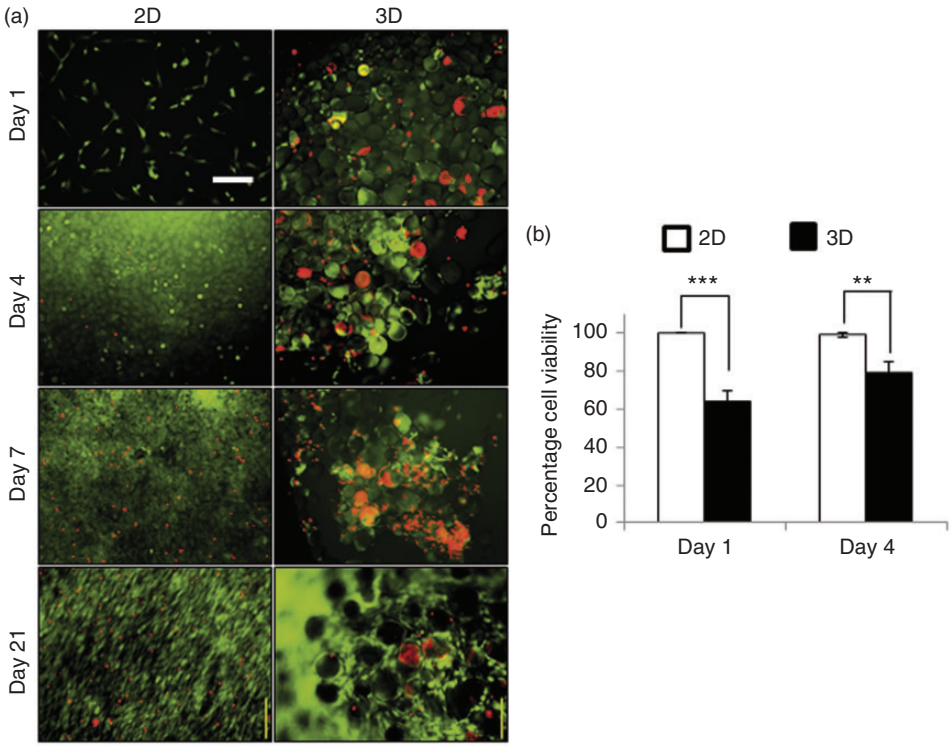

Figure 4. Viability of human mesenchymal stem cells in 2D and 3D. (a) Overlay of FITC/Texas Red channels images for days 1, 4, 7 and 21 of culture. (b) Percentage cell viability in 2D and 3D after 1 and 4 days of culture was calculated using image analysis by quantifying the pixels for green (live) and red (dead) signal. $^{**}p < 0.01$ and $^{***}p < 0.001$, $n \geq 4$. Error bars represent S.E.M. Scale bar – 200 μm.

to (d). These images show thick cell layers (>2 layers thick) surrounding the agglomerate. However, when this agglomerate was split, there were more cells present near the edges as compared to the central (internal) regions of the agglomerate, which suggested heterogeneity in hMSC colonisation across the 3D sample. Similar observations were also made after H&E staining of cryosectioned 3D cultures (see Supplementary Figure 2(a)). SEM images also indicated presence of more cells in inter-particulate region and relatively fewer cells present directly in contact with the surface of BSG, where they acquired either a flat or a rounded morphology, see Figure 3(e) and (f). This again suggested heterogeneity in cell distribution within the same 3D sample.

Cell viability

To determine whether the difference in DNA content and metabolic profile in 2D and 3D may be due to differences in cell viability, hMSCs were seeded at 2500 cell/cm^2 and FDA/PI staining was performed over three weeks of culture. The results (Figure 4(a) and (b)) showed significantly higher proportion of dead cells in 3D compared to 2D on day 1 ($p < 0.001$) and day 4 ($p < 0.01$) and the same was also observed qualitatively on day 7. However, by the end of 21 days of culture, the proportion of viable cells seemed to have improved in 3D and very few dead cells were observed.

Alkaline phosphatase activity

To evaluate changes in differentiation response, ALP activity was measured in 2D and 3D, GFP-labelled hMSCs were seeded at higher cell seeding density of 10,000 cells/cm^2 [30] and measurements were taken over three weeks of culture in SC and OS media. The results (Figure 5) showed that hMSCs increased ALP activity in response to OS medium in both 3D and 2D cultures, compared to respective SC medium cultures ($p < 0.001$). Also, there was higher ALP activity in OS-treated cells in 3D cultures compared to 2D cultures on day 7, 14 and 21.

Collagen production

To assess collagen production in 2D and 3D, GFP-labelled hMSCs were seeded at 10,000 cells/cm^2 and Sirius Red staining was performed after three weeks of culture in SC and OS media (Figure 6(a)). OS treatment led to more intense collagen staining in 2D cultures compared to SC medium on day 21 of

differentiation. In 3D cultures, cryosectioned samples showed the presence of red-coloured spots indicating collagen production in both OS and SC conditions.

Quantitative results (see Figure 6(b)) showed significantly higher collagen in 2D cultures under OS treatment than SC medium on day 7 ($p < 0.01$) and day 21 ($p < 0.001$) of differentiation. However, in case of 3D cultures, there was no difference between OS and SC conditions on day 7 of differentiation. Moreover, there was also higher reading in 3D SC compared to 3D OS by day 21 ($p < 0.001$) due to significant drop in staining for 3D OS samples between day 7 and day 21 ($p < 0.01$).

Comparison of 2D and 3D showed significantly higher staining in 3D SC compared to 2D SC on day 7 ($p < 0.01$). However, by day 21, there was nine and four times more staining in 2D OS and 2D SC conditions relative to 3D OS and 3D SC conditions, respectively ($p < 0.001$).

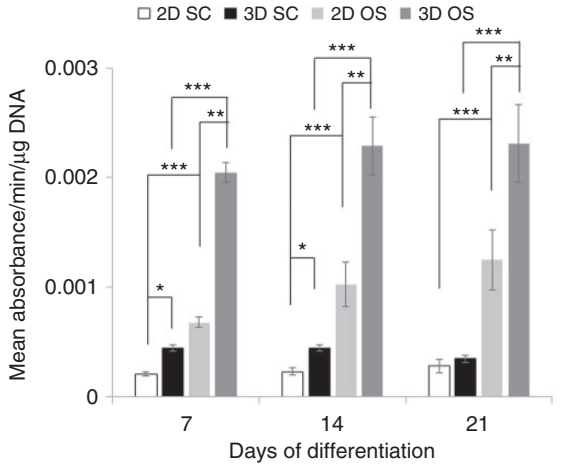

Figure 5. Alkaline phosphatase activity measurements of human mesenchymal stem cells in 2D and 3D culture in standard culture medium and osteogenic medium over 21 days, normalised to DNA content. Cells were seeded at 10,000 cells/cm^2. ***, ** and * indicate $p < 0.001$, $p < 0.01$ and $p < 0.05$, respectively, n = 3, error bars represent S.E.M.

Calcium deposition

To assess the extent of mineral deposition in 2D and 3D, GFP-labelled hMSCs were seeded at 10,000 cells/cm^2 and Alizarin Red staining was performed after three weeks culture in SC and OS medium. Figure 7(a) shows Alizarin Red stained cells in two culture formats after 7 and 21 days of differentiation. On day 7, cells in 2D condition did not show positive calcium staining but by day 21, there was presence of intense positive mineral staining in 2D OS. In 3D cultures, patchy stained regions were observed in both 3D OS and 3D SC conditions on day 7 as well as day 21 of differentiation, suggesting the influence of 3D geometry on hMSC response. Similar observation was also made through H&E stained 3D cryosections on day 21 (see Supplementary Figure 2(b)).

The results for quantitative assessment (Figure 7(b)) showed significantly higher values in 2D compared to 3D in both media. As expected, 2D cultures under OS treatment had significantly higher staining as compared to those under SC conditions. However, in the case of 3D, no statistically significant difference was seen between OS and SC conditions after 21 days of treatment, suggesting that induction medium did not enhance mineral deposition in 3D geometry.

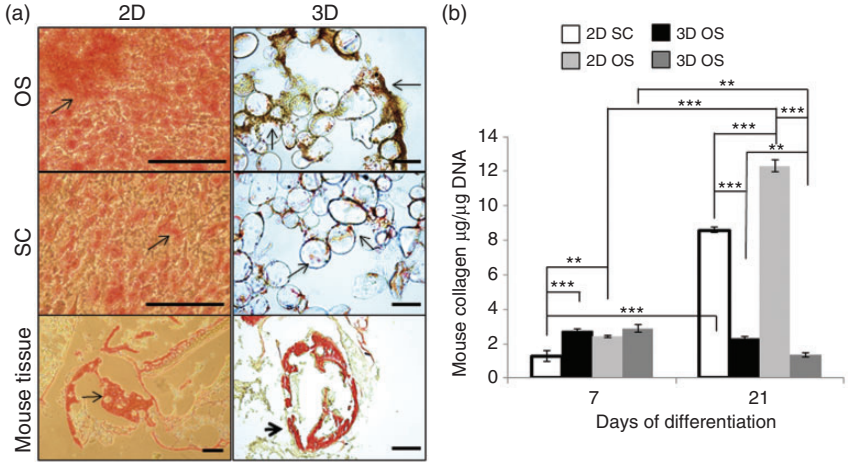

Figure 6. Collagen staining in human mesenchymal stem cells maintained in 2D and 3D cultures in standard culture medium and osteogenic medium over 21 days. (a) Sirius Red staining indicating the presence of collagen (arrows) at day 21. Mouse calvarial tissue was used as a positive control for staining. (b) Quantitative assessment of collagen staining at day 7 and day 21. *** and ** indicate $p < 0.001$ and $p < 0.01$, respectively, n = 3, error bars represent S.E.M. Scale bar – 100 µm.

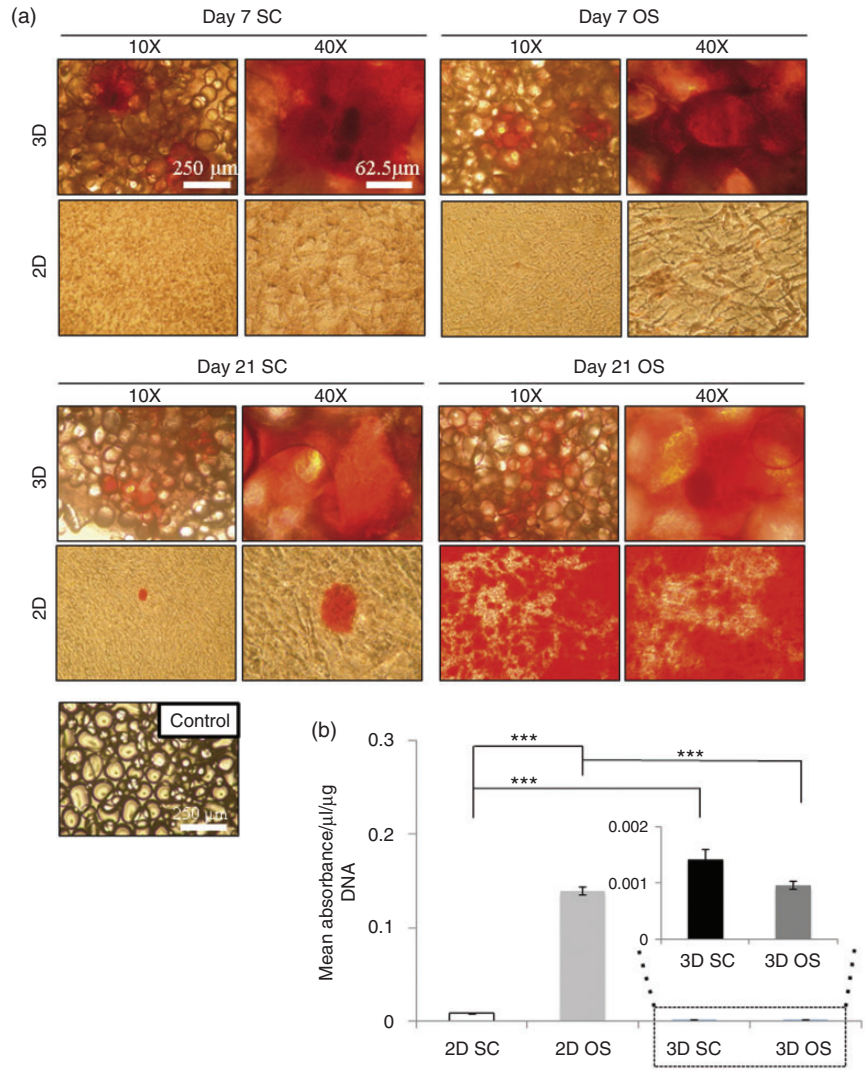

Figure 7. Alizarin Red staining of human mesenchymal stem cultures in 2D and 3D maintained in standard culture medium and osteogenic medium for 21 days after cell seeding at 10,000 cells/cm^2. (a) Staining images taken on day 7 and 21 of differentiation. BSG stained without cells were used as a negative control. (b) Quantitative assessment of staining on day 21 of differentiation. *** and ** indicate $p < 0.001$ and $p < 0.01$, respectively, n = 3, error bars represent S.E.M.

Discussion

Metabolic differences exist in 2D and 3D

In this study, hMSC growth, viability and osteogenic response were compared on 2D and 3D geometries, using MS of known radii of curvature, in order to evaluate geometrical control of hMSC fate.

It was expected that with increasing DNA content there would be a proportional increase in cell metabolic activity in 3D, similar as is seen is 2D. However, there was no linear correlation between cell metabolic activity and DNA content in 3D in extended culture periods. Similar observations have also been reported by Ng et al.,[31] who showed that Cell Titer 96, [^{3}H] thymidine and Alamar Blue assays provided an inaccurate measure of human dermal fibroblast numbers in contrast to DNA assay and cell counts, over 10 days culture period in 3D poly(lactic-co-glycolic) acid-poly(ε-caprolactone) (PLGA-PCL) mesh containing 80 µm-wide PCL fibers and 20 µm-wide PLGA fibers, which provided similar radii of curvatures as used in the current study.

Additionally, some studies have shown that mitochondrial metabolism in 2D and 3D may be different. For example, almost 50–60% down regulation in mitochondrial enzymes (involved in oxidative phosphorylation) and 50–60% upregulation in anaerobic glycolysis was seen in case of human liver cancer cells grown on collagen scaffolds (Lyostypt® from B. Braun, Germany, collagen type I as major constituent and with 10–25 µm approx. radii of curvature) as compared to

monolayers.[32] This indicates that cells in 2D and 3D may have different metabolism and therefore, extrapolating cell numbers in 3D samples using 2D standard curves may provide an inaccurate measure of cell proliferation in 3D, as done by some studies using titanium phosphate-based glass MS for MG63 cell culture[16] and collagen-apatite MS for rat bone marrow derived MSC culture.[33] Moreover, these topographically-based differences may not be limited to mitochondrial metabolism but may also be affecting other cellular processes such as osteogenic differentiation as demonstrated by Maeno et al.[11]

Geometrical regulation of hMSC survival and fate

Some studies have demonstrated that cells are able to sense the radii of curvature smaller or much larger than the size of the cells themselves affecting cell attachment[34,35] migration,[36–38] growth[39–44] and differentiation.[45–50] Where concave surfaces in 3D support cell growth, convex or flat surfaces in same 3D system can inhibit it.[42,43] There is also evidence that the level of concavity can dictate rate of cell growth and ECM deposition.[49] At the molecular level, it is suggested that once the curvature-sensing proteins and lipids in plasma membrane sense the local curvature of adhesion surface, they accumulate themselves in the regions of membrane that needs to be bended, thus inducing a local membrane curvature. This curved membrane region causes a physical tension on plasma membrane via the integrin-focal adhesion proteins-actomyosin fibers-RhoA assembly, affecting the signalling pathways involved in osteogenic differentiation and survival.[51–56]

In the present study, MS ranged between 8 and 270 μm in diameter with mean and S.D. of 90 μm and 47 μm, respectively (Supplementary Figure 1) and they presented the cells with a range of radii of curvatures between 4-130 μm. Thus, it is possible that different regions of the same 3D agglomerate may have led to different cell-fates (see Supplementary Figure 3(a)). The regions with high convexities (sharper edges on MS surfaces) may have induced high cytoskeletal-mediated tension on the plasma membrane, leading to damage and ultimately cell death in some cells. In other cells, reduced cell membrane integrity may have negatively affected cellular processes, such as cell division and cell migration, limiting their growth[57] (see Supplementary Figure 3(b) to (d)). This may explain significantly reduced cell viability on MS as compared to flat 2D surface and therefore, reduced cell proliferation in 3D.

The Supplementary Table 1 summarises results from some previous studies reporting growth of different cell-types on different MS systems with similar radii of curvature as BSG. Though most of these studies do not clearly define the cell seeding density with respect to surface area, there seems to be a general trend of significantly reduced cell proliferation in MS culture as compared to monolayers, irrespective of the chemical composition of MS, of the culture medium used[33,58–60] or of the surface area offered by MS. This suggests that convex surfaces in general may be limiting cell growth.[43]

Recently, it has been shown that cells may be able to adapt to physical stresses in their environment by distributing proliferative activity and integrating the mechanical equilibrium through cell–cell adhesion and communication, spread across layers of cells.[61–63] This suggests that hMSCs may be able to develop a growth pattern such that they collectively overcome harsher convexities of MS. This may explain the presence of viable cells in 3D on day 21 of culture in the present study. Similar observations have also been reported for human osteocytes grown on angular particles (60% hydroxyapatite and 40% of β-tricalcium phosphate, 20–40 μm radii of curvature) where there was 70% and 99% viability after 20 h and 28 days of culture, respectively.[64]

Live cell images, SEM images and H&E staining also showed that cells tend to grow and form aggregates predominantly in the inter-particulate spaces or at the outer edges of 3D agglomerates. This MS aggregation has also been reported for a range of MS including Ti-doped phosphate based glass MS,[59] collagen or collagen-apatite MS[33] and commercially available Cytodex 1, Cytodex 3, Cultispher GL and HyQsphere P102-L MC,[65] all in comparable size range of BSG, hinting that aggregation may be primarily due to MS 3D geometry rather than their composition. One possible explanation for this may be the reduced physical tension experienced by the cells in inter-particulate porosity, (see Supplementary Figure 3(d) and (e)) and flatter regions (in the outer edges of the same agglomerate), which may have allowed these cells to grow more rapidly as compared to cells spread over convex MS surfaces. Additionally, pores may have different patterns of cell colonisation due to their different sizes,[62] which could lead to formation of heterogonous growth microenvironments within the same 3D sample. Some optimal-sized pores may have been more osteoinductive than others and led to the deposition of ECM and mineral by differentiated MSCs.[49] Hence, giving it a patchy appearance on as early as day 7, even without osteogenic supplements. At the same time, the addition of osteogenic factors unexpectedly fail to significantly enhance collagen or calcium deposition in 3D cultures. These results suggest that geometry rather than medium composition may play a leading role in osteogenic differentiation[52,55] and would support some previous *in vivo* studies which have also shown preferential mineralisation on concave surfaces of implants rather than convex features in osteogenic sites[48] as well as ectopic sites.[66]

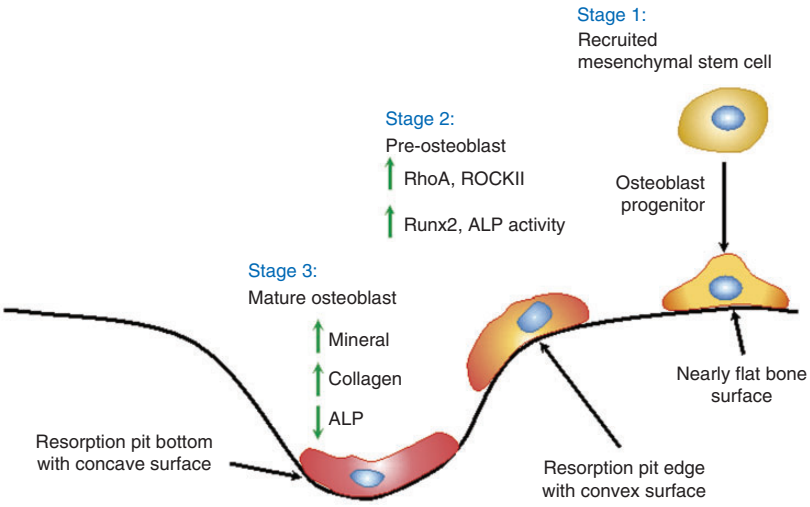

Figure 8. Proposed model for geometrical regulation of bone formation, based on contributions also from literature.[49,56,67,68,73] ROCK: Rho-associated protein kinase, ALP: alkaline phosphatase.

Our results also showed significantly higher ALP activity in 3D than in 2D. This may be due to acto-myosin contractility in cells as a result of 3D geometry, which may have enhanced RhoA expression and ROCKII activation, leading to increased ALP activity.[56,67,68] Similar results have also been reported for pre-osteoblast (MC3T3) cells cultured on CaP cement-alginate MS with 75–150 µm radii of curvature (similar to BSG) and <5 µm pore size on surface (absent on BSG) in osteogenic differentiation medium after 14 days.[69]

However, despite higher ALP activity, lower collagen and calcium deposition were observed in 3D as compared to 2D; this was also reported in case of MSCs derived from dental pulp, which had higher ALP activity (after 48 h culture) but lower osteocalcin, osteonectin and BSP expression (after 30 days culture) on hydroxyapatite-convex surfaces (150 µm wide chips) compared to PLGA-concave surfaces (20–50 µm radii of curvature with micro-pits 3–10 µm wide) and Ti-flat surfaces.[70]

Considering that BSG used in this study did not provide MSCs with any specific osteoinductive chemistry or nanotopography, it seems that their convex surfaces and the resulting 3D geometry of adherent cells may have been sufficient to induce ALP expression in MSCs, but not late osteogenesis stages. This may be linked to the physiological environment in which these cells have been typically shown to form bone inside the resorption pits, which probably offer concave and not convex surfaces.[71,72]

Based on this hypothesis, a model for geometrical control of osteogenesis *in vivo* may be proposed (Figure 8): in *Stage 1* (osteoblast progenitor stage), MSCs may be recruited for bone formation on relatively flat bone surface where they may attach and migrate towards the resorption pit created by osteoclasts. During migration in *Stage 2* (pre-osteoblast stage), these cells initially encounter the convex edges of concavity (resorption pits), which may cause actin-myosin contractility and cytoskeleton-tension, inducing early osteogenesis through RhoA-ROCKII-Runx2/ALP pathway. Finally, as these cells enter the concavity in *Stage 3* (mature osteoblast stage), they may experience a concave topography, which may induce different cytoskeletal changes and subsequent molecular pathways, promoting the formation of collagen fibers and mineralised bone matrix.

It should be noted that the chemical composition of glass coverslips used might present slight differences from that of the BSG used, as they were from different sources. Although the present study focused on the dominant effect of topography and geometry on cell fate[55] in 2D and 3D, in the future this may be tested by manufacturing glass coverslips and BSG from the same the glass raw materials, and comparing hMSC growth and differentiation on their surfaces.

Conclusion

This study explored hMSC responses in 2D and MS (3D) culture systems, and showed lower cell viability in 3D and also lower cell proliferation in 3D over 6 weeks. Microscopic examination indicated that the cells tended to populate in inter-particulate spaces and fewer cells grew on MS surfaces. There was higher ALP activity in 3D over 21 days of culture, however, collagen and calcium deposition was found to be significantly lower after 3 weeks of 3D culture compared to standard 2D culture. When culture medium was supplemented with osteogenic factors,

the ALP activity seemed to increase in both 2D and 3D, while collagen and mineral deposition did not seem to increase upon OS treatment in 3D. These differences between the two culture formats may be due to variation in cell morphology resulting from cytoskeletal changes induced by convex MS-surfaces and inter-particulate regions in the 3D system. Based on these observations, a model for geometrical regulation of osteogenesis by hMSCs was proposed. Future work will focus on understanding how cell morphology modulates cell contractility and how this cytoskeletal tension transduces into molecular signals, possibly leading to osteogenesis.

Acknowledgements

The authors are thankful to Mrs. Denise Mclean for guidance with histology and Dr. Glen Kirkham for providing the mouse tissue.

Author Contributions

D.G. performed BSG characterisations, cell-based experiments, analysed data and prepared the manuscript. K.M.Z.H. and I.A. were responsible for microsphere manufacturing. D.M.G. and V.S. were responsible for overall project supervision, study design and analysis.

Declaration of Conflicting Interests

The author(s) declared no potential conflicts of interest with respect to the research, authorship and/or publication of this article.

Funding

The author(s) disclosed receipt of the following financial support for the research, authorship, and/or publication of this article: This work was supported by Vice Chancellor's Scholarship for Excellence in Research from University of Nottingham, and also support from the European Union's Seventh Framework Programme (FP7/2007–2013) under grant agreement no. 263363.

Supplementary material

Supplementary material is available for this article online.

References

1. Tang Y, Wu X, Lei W, et al. TGF- β1-induced migration of bone mesenchymal stem cells couples bone resorption with formation. *Nat Med* 2009; 15: 757–765.
2. Walters NJ and Gentleman E. Evolving insights in cell-matrix interactions: elucidating how non-soluble properties of the extracellular niche direct stem cell fate. *Acta Biomater* 2015; 11: 3–16.
3. Evans EA and Calderwood DA. Forces and bond dynamics in cell adhesion. *Science* 2007; 316: 1148–1153.
4. Harburger DS and Calderwood DA. Integrin signalling at a glance. *J Cell Sci* 2009; 122: 159–163.
5. Baker BM and Chen CS. Deconstructing the third dimension – how 3D culture microenvironments alter cellular cues. *J Cell Sci* 2012; 125: 3015–3024.
6. Abbott A. Cell culture: biology's new dimension. *Nature* 2003; 424: 870–872.
7. Lutolf MP, Gilbert PM and Blau HM. Designing materials to direct stem-cell fate. *Nature* 2009; 462: 433–441.
8. Wang F, Weaver VM, Petersen OW, et al. Reciprocal interactions between beta1-integrin and epidermal growth factor receptor in three-dimensional basement membrane breast cultures: a different perspective in epithelial biology. *Proc Natl Acad Sci U S A* 1998; 95: 14821–14826.
9. Sung KE, Su X, Berthier E, et al. Understanding the impact of 2D and 3D fibroblast cultures on in vitro breast cancer models. *PLoS One* 2013; 8: e76373.
10. Petrie RJ and Yamada KM. Fibroblasts lead the way: a unified view of 3D cell motility. *Trends Cell Biol* 2015; 25:666–674.
11. Maeno S, Niki Y, Matsumoto H, et al. The effect of calcium ion concentration on osteoblast viability, proliferation and differentiation in monolayer and 3D culture. *Biomaterials* 2005; 26: 4847–4855.
12. Malda J and Frondoza CG. Microcarriers in the engineering of cartilage and bone. *Trends Biotechnol* 2006; 24: 299–304.
13. Kim KK and Pack DW. Microspheres for drug delivery. *BioMEMS Biomed Nanotechnol* 2006; 19–50. Springer US.
14. Park JH, Pérez RA, Jin GZ, et al. Microcarriers designed for cell culture and tissue engineering of bone. *Tissue Eng Part B Rev* 2013; 19: 172–190.
15. Hossain KMZ, Patel U and Ahmed I. Development of microspheres for biomedical applications: a review. *Prog Biomater* 2015; 4: 1–9.
16. Lakhkar NJ, Park JH, Mordan NJ, et al. Titanium phosphate glass microspheres for bone tissue engineering. *Acta Biomater* 2012; 8: 4181–4190.
17. Li M, Wilkinson D and Patchigolla K. Comparison of particle size distributions measured using different techniques. *Part Sci Technol* 2005; 23: 265–284.
18. Manikandan S, Jagannath, Shrikhande VK, et al. Degradation behaviour of borosilicate glass: some studies. *Anti-Corros Methods Mater* 2006; 53: 303–309.
19. Hoppe A, Güldal NS and Boccaccini AR. A review of the biological response to ionic dissolution products from bioactive glasses and glass-ceramics. *Biomaterials* 2011; 32: 2757–2774.
20. Okamoto T, Aoyama T, Nakayama T, et al. Clonal heterogeneity in differentiation potential of immortalized human mesenchymal stem cells. *Biochem Biophys Res Commun* 2002; 295: 354–361.
21. Rashidi H, Strohbuecker S, Jackson L, et al. Differences in the pattern and regulation of mineral deposition in human cell lines of osteogenic and non-osteogenic origin. *Cells Tissues Organs* 2012; 195: 484–494.
22. France LA, Scotchford CA, Grant DM, et al. Transient serum exposure regimes to support dual differentiation of human mesenchymal stem cells. *J Tissue Eng Regen Med* 2012; 8: 652–663.

23. Harrison R, Markides H, Morris RH, et al. Autonomous magnetic labelling of functional mesenchymal stem cells for improved traceability and spatial control in cell therapy applications. *J Tissue Eng Regen Med* 2017; 11: 2333–2348.
24. Kuroda Y, Wakao S, Kitada M, et al. Isolation, culture and evaluation of multilineage-differentiating stress-enduring (Muse) cells. *Nat Protoc* 2013; 8: 1391–1415.
25. Ahmadi R, Mordan N, Forbes A, et al. Enhanced attachment, growth and migration of smooth muscle cells on microcarriers produced using thermally induced phase separation. *Acta Biomater* 2011; 7: 1542–1549.
26. Shi X, Jiang J, Sun L, et al. Hydrolysis and biomineralization of porous PLA microspheres and their influence on cell growth. *Colloids Surf B Biointerfaces* 2011; 85: 73–80.
27. Lareu RR, Zeugolis DI, Abu-Rub M, et al. Essential modification of the Sircol Collagen assay for the accurate quantification of collagen content in complex protein solutions. *Acta Biomater* 2010; 6: 3146–3151.
28. Kliment CR, Englert JM, Crum LP, et al. A novel method for accurate collagen and biochemical assessment of pulmonary tissue utilizing one animal. *Int J Clin Exp Pathol* 2011; 4: 349–355.
29. Abou Neel EA, Mizoguchi T, Ito M, et al. In vitro bioactivity and gene expression by cells cultured on titanium dioxide doped phosphate-based glasses. *Biomaterials* 2007; 28: 2967–2977.
30. Jaiswal N, Haynesworth SE, Caplan AI, et al. Osteogenic differentiation of purified, culture-expanded human mesenchymal stem cells in vitro. *J Cell Biochem* 1997; 64: 295–312.
31. Ng KW, Leong DTW and Hutmacher DW. The challenge to measure cell proliferation in two and three dimensions. *Tissue Eng* 2005; 11: 182–191.
32. Pruksakorn D, Lirdprapamongkol K, Chokchaichamnankit D, et al. Metabolic alteration of HepG2 in scaffold-based 3-D culture: proteomic approach. *Proteomics* 2010; 10: 3896–3904.
33. Kim HW, Gu HJ and Lee HH. Microspheres of collagen-apatite nanocomposites with osteogenic potential for tissue engineering. *Tissue Eng* 2007; 13: 965–973.
34. Itoga K, Yamato M, Kobayashi J, et al. Cell micropatterning using photopolymerization with a liquid crystal device commercial projector. *Biomaterials* 2004; 25: 2047–2053.
35. Elliott H, Fischer RS, Myers KA, et al. Myosin II controls cellular branching morphogenesis and migration in three dimensions by minimizing cell-surface curvature. *Nat Cell Biol* 2015; 17: 137–147.
36. Park JY, Lee DH, Lee EJ, et al. Study of cellular behaviors on concave and convex microstructures fabricated from elastic PDMS membranes. *Lab Chip* 2009; 9: 2043–2049.
37. Kim MH, Sawada Y, Taya M, et al. Influence of surface topography on the human epithelial cell response to micropatterned substrates with convex and concave architectures. *J Biol Eng* 2014; 8: 13.
38. de Vicente G and Lensen MC. Topographically and elastically micropatterned PEG-based hydrogels to control cell adhesion and migration. *Eur Polym J* 2016; 78: 290–301.
39. Wan Y, Wang Y, Liu Z, et al. Adhesion and proliferation of OCT-1 osteoblast-like cells on micro- and nano-scale topography structured poly(L-lactide). *Biomaterials* 2005; 26: 4453–4459.
40. Zhang LG, Zhong DH, Zhang Y, et al. A microwell pattern for c17.2 cell aggregate formation with concave cylindrical surface induced cell peeling. *Biomaterials* 2014; 35: 9423–9437.
41. Bigerelle M, Giljean S and Anselme K. Existence of a typical threshold in the response of human mesenchymal stem cells to a peak and valley topography. *Acta Biomater* 2011; 7: 3302–3311.
42. Bidan CM, Kommareddy KP, Rumpler M, et al. How linear tension converts to curvature: geometric control of bone tissue growth. *PLoS One* 2012; 7: e36336.
43. Rumpler M, Woesz A, Dunlop JWC, et al. The effect of geometry on three-dimensional tissue growth. *J R Soc Interface* 2008; 5: 1173–1180.
44. Bidan CM. *Geometric control of tissue growth and organisation*, PhD Thesis, Max-Planck-Institut of Colloids and Interfaces, Germany, 2013.
45. Dalby MJ, Gadegaard N, Tare R, et al. The control of human mesenchymal cell differentiation using nanoscale symmetry and disorder. *Nat Mater* 2007 Dec; 6: 997–1003.
46. Ball M, Grant DM, Lo WJ, et al. The effect of different surface morphology and roughness on osteoblast-like cells. *J Biomed Mater Res Part A* 2008; 86: 637–647.
47. Li Z, Gong Y, Sun S, et al. Differential regulation of stiffness, topography, and dimension of substrates in rat mesenchymal stem cells. *Biomaterials* 2013; 34: 7616–7625.
48. Scarano A, Degidi M, Perrotti V, et al. Experimental evaluation in rabbits of the effects of thread concavities in bone formation with different titanium implant surfaces. *Clin Implant Dent Relat Res* 2014; 16: 572–581.
49. Bidan CM, Kollmannsberger P, Gering V, et al. Gradual conversion of cellular stress patterns into prestressed matrix architecture during in-vitro tissue growth. *J R Soc Interface* 2016; 13.
50. Werner M, Blanquer SBG, Haimi SP, et al. Surface curvature differentially regulates stem cell migration and differentiation via altered attachment morphology and nuclear deformation. *Adv Sci* 2017; 4.
51. McMahon HT and Gallop JL. Membrane curvature and mechanisms of dynamic cell membrane remodelling. *Nature* 2005; 438: 590–596.
52. McBeath R, Pirone DM, Nelson CM, et al. Cell shape, cytoskeletal tension, and RhoA regulate stem cell lineage commitment. *Dev Cell* 2004; 6: 483–495.
53. Vogel V and Sheetz M. Local force and geometry sensing regulate cell functions. *Nat Rev Mol Cell Biol* 2006; 7: 265–275.
54. Graham TR and Kozlov MM. Interplay of proteins and lipids in generating membrane curvature. *Curr Opin Cell Biol* 2010; 22: 430–436.

55. Kilian KA, Bugarija B, Lahn BT, et al. Geometric cues for directing the differentiation of mesenchymal stem cells. *Proc Natl Acad Sci U S A* 2010; 107: 4872–4877.
56. Ozdemir T, Xu LC, Siedlecki C, et al. Substrate curvature sensing through Myosin IIa upregulates early osteogenesis. *Integr Biol Camb* 2013; 5: 1407–1416.
57. Binamé F, Pawlak G, Roux P, et al. What makes cells move: requirements and obstacles for spontaneous cell motility. *Mol Biosyst* 2010; 6: 648–661.
58. Hong SJ, Yu HS and Kim HW. Tissue engineering polymeric microcarriers with macroporous morphology and bone-bioactive surface. *Macromol Biosci* 2009; 9: 639–645.
59. Guedes JC, Park JH, Lakhkar NJ, et al. TiO_2-doped phosphate glass microcarriers: a stable bioactive substrate for expansion of adherent mammalian cells. *J Biomater Appl* 2013; 28: 3–11.
60. Barrias CC, Ribeiro CC and Barbosa MA. Adhesion and proliferation of human osteoblastic cells seeded on injectable hydroxyapatite microspheres. *Key Eng Mater* 2004; 254–256: 877–80.
61. Nelson CM, Jean RP, Tan JL, et al. Emergent patterns of growth controlled by multicellular form and mechanics. *Proc Natl Acad Sci U S A* 2005; 102: 11594–11599.
62. Kollmannsberger P, Bidan CM, Dunlop JWC, et al. The physics of tissue patterning and extracellular matrix organisation: how cells join forces. *Soft Matter* 2011; 7: 9549–9560.
63. Bidan CM, Wang FM and Dunlop JWC. A three-dimensional model for tissue deposition on complex surfaces. *Comput Methods Biomech Biomed Eng* 2013; 16: 1056–1070.
64. Boukhechba F, Balaguer T, Michiels J-F, et al. Human primary osteocyte differentiation in a 3D culture system. *J Bone Miner Res* 2009; 24: 1927–1935.
65. Goh TK, Zhang ZY, Chen AKL, et al. Microcarrier culture for efficient expansion and osteogenic differentiation of human fetal mesenchymal stem cells. *Biores Open Access* 2013; 2: 84–97.
66. Ripamonti U. Biomimetism, biomimetic matrices and the induction of bone formation. *J Cell Mol Med* 2009; 13: 2953–2972.
67. Hansen JC, Lim JY, Xu LC, et al. Effect of surface nanoscale topography on elastic modulus of individual osteoblastic cells as determined by atomic force microscopy. *J Biomech* 2007; 40: 2865–2871.
68. Seo CH, Furukawa K, Montagne K, et al. The effect of substrate microtopography on focal adhesion maturation and actin organization via the RhoA/ROCK pathway. *Biomaterials* 2011; 32: 9568–9575.
69. Park JH, Lee EJ, Knowles JC, et al. Preparation of in situ hardening composite microcarriers: calcium phosphate cement combined with alginate for bone regeneration. *J Biomater App* 2014; 28: 1079–1084.
70. Graziano A, d'Aquino R, Cusella-De Angelis MG, et al. Concave pit-containing scaffold surfaces improve stem cell-derived osteoblast performance and lead to significant bone tissue formation. *PLoS One* 2007; 2: e496.
71. Teitelbaum SL and Ross FP. Genetic regulation of osteoclast development and function. *Nat Rev Genet* 2003; 4:638–649.
72. Florencio-Silva R, Sasso GR, Sasso-Cerri E, et al. Biology of bone tissue: structure, function, and factors that influence bone cells. *Biomed Res Int* 2015; 2015.
73. Graziano A, d'aquino R, Cusella-De Angelis MG, et al. Scaffold's surface geometry significantly affects human stem cell bone tissue engineering. *J Cell Physiol* 2008; 214: 166–172.